Journal of Translational Medicine

RESEARCH

Open Access

Depleting parenchymal border macrophages alleviates cerebral edema and neuroinflammation following status epilepticus

Renbao Lin[1], Rui Luo[2], Xinyue Yu[1], Junjie Zou[1*], Xiaowei Huang[3*] and Yanwu Guo[1*]

Abstract

Background Status epilepticus (SE) is a common severe neurological emergency. Cerebral edema caused by SE is unavoidable and may exacerbate epilepsy. Recent studies have identified cerebrospinal fluid (CSF) as a crucial fluid source of initial cerebral edema following ischemic stroke and cardiac arrest. Moreover, synchronized neuronal firings drive CSF influx into interstitial fluid (ISF). Parenchymal border macrophages (PBMs) have been found to play a role in regulating CSF flow dynamics. However, the involvement of CSF and PBMs in cerebral edema during SE remains unclear. Here, we investigated the fluid source of cerebral edema in the initial phase of SE with the role of PBMs involved.

Methods Lithium chloride-pilocarpine was used to induce SE in C57BL/6 J mice. Electroencephalogram (EEG) was acquired to assess changes in relative EEG power pre- and post-seizure onset. Apparent diffusion coefficient (ADC) maps reconstructed from diffusion-weighted imaging (DWI) were utilized to evaluate cytotoxic edema. Blood–brain barrier (BBB) permeability was examined using sodium fluorescein (NaFl). CSF tracer influx into the brain was assessed by transcranial imaging and brain slices. PBMs were depleted using clodronate liposomes. Immunohistochemistry was used to evaluate PBM depletion, severity of vasogenic edema, inflammation, and neuronal damage.

Results During the initial stage of SE, relative EEG power sharply increased and ADC values significantly decreased. Concurrently, CSF tracer influx into the cortex significantly elevated, though NaFl leakage from blood to brain parenchyma did not evidently alter. Following depletion of PBM, CSF influx declined but AQP4 expression and polarization remained unaffected. Post-PBM depletion, there was no significant alteration in relative EEG power, yet CSF influx decreased substantially during the initial stage of SE. The degree of ADC decline lessened, IgG extravasation after SE decreased, activated microglia and proliferating astrocytes count fell, and neuronal damage post-SE alleviated.

Conclusions CSF appeared to contribute to cerebral edema in SE. Depletion of PBM alleviated cytotoxic edema in the initial phase of SE, and subsequent vasogenic edema, inflammatory response and neurological damage were reduced. These findings may provide potential novel strategies for treating cerebral edema following SE.

*Correspondence:
Junjie Zou
angzoujj@163.com
Xiaowei Huang
huangxw@dgut.edu.cn
Yanwu Guo
eguoyanwu@163.com
Full list of author information is available at the end of the article

Keywords Parenchymal border macrophage (PBM), Cerebral edema, Cerebrospinal fluid (CSF), Blood–brain barrier (BBB), Status epilepticus (SE), Inflammation

Introduction

Status epilepticus (SE), occurring in 10–41 per 100,000 people annually, is a common neurological emergency that can result in permanent pathological injury or even mortality [1, 2]. Cerebral edema is inevitable in SE, as evidenced by abnormal diffusion-weighted imaging (DWI) signals in the cortex, hippocampus, amygdala, thalamus, and other areas of clinical epileptic patients and animal models, indicating edema at multiple sites [3, 4]. Cerebral edema exacerbates secondary brain injury, including cell death, inflammatory response, and blood–brain barrier disruption. These pathological processes form a positive feedback loop that modulates neuronal hyperexcitability and reduces seizure threshold, promoting epileptogenesis [5–7]. Therefore, mitigating cerebral edema is one of the primary therapeutic strategies for SE, as it could help to improve the prognosis of patients.

There are three distinct phases in the development of cerebral edema. Firstly, cytotoxic edema is the key initial step and driving factor, where dysfunction of the Na^+/K^+-ATPase and imbalanced transmembrane ion gradients lead to cell swelling; subsequently, cytotoxic edema generates new ion gradients across the blood–brain barrier (BBB), allowing Na^+ and water to accumulate through the BBB, constituting the ionic edema stage; finally, the previous stages cause astrocytes and vascular endothelial cells swelling and loss of normal morphology, damaging BBB integrity and permitting plasma proteins and water leakage into the brain tissue [8]. However, recent research has found that cerebrospinal fluid (CSF) serves as a primary source of Na^+ and water in early cerebral edema after ischemic strokes and cardiac arrests, with CSF and interstitial fluid (ISF) exchange providing a pathway [9, 10]. Additionally, a newer study discovered that neuronal synchronized discharges drive CSF influx into the ISF [11]. However, the role of CSF in cerebral edema development during SE remains unknown.

In recent years, increasing attention has been paid to parenchymal border macrophages (PBMs), also known as central nervous system (CNS) border-associated macrophages (BAMs). As a resident myeloid cell population distinct from microglia, PBMs are distributed in the perivascular spaces (PVS) and leptomeninges [12, 13]. However, their precise roles in the CNS remain to be fully explored. Previous studies have shown that these macrophages are closely associated with the pathogenesis of CNS diseases. They exhibit protective effects in bacterial meningitis and Alzheimer's disease (AD) [14–16], but can also increase BBB permeability and play harmful roles in chronic hypertension, stroke, and experimental autoimmune encephalomyelitis [17–19]. Recent research has revealed the critical function of PBMs in regulating CSF flow dynamics—their depletion can reduce CSF influx into brain parenchyma [20]. This provides deeper insight into PBM functions in neurologic disorders. Given their location and functions, we hypothesize that PBMs may play an important role in the development of cerebral edema.

In this study, we found that CSF is an important fluid source contributing to cerebral edema in the initial stage of SE. Depletion of PBM mitigated cerebral edema, inflammatory response and neurological injury in mice after SE. These findings may provide a potential novel therapeutic approach for cerebral edema following SE.

Methods

Animals

The Animal Ethics Committee of Zhujiang Hospital of Southern Medical University approved all experimental protocols. The Guide for the Care and Use of Laboratory Animals published by the National Institutes of Health of the United States was followed for all animal experiments. Male C57BL/6 J mice of 8 weeks of age were acquired from the Hunan SJA Laboratory Animal Co., Ltd. Mice were housed in 12 h dark/light cycle at a stable temperature with free access to water and food. In this study, a total of 254 mice were used, with 25 excluded due to experimental failure or bleeding after cisterna magna cannulation. Among the 170 mice used for SE modeling, 58 died. An additional 2 mice died during transcranial imaging experiments.

Induction of SE

Mice were injected intraperitoneally with lithium chloride (423 mg/kg, i.p.; Sigma-Aldrich) 20 h prior to the treatment of pilocarpine (40 mg/kg, i.p.; Sigma-Aldrich). To reduce the peripheral effects of pilocarpine, methylscopolamine (1 mg/kg, i.p.; Shanghai Aladdin Biochemical Technology Co., Ltd.) was administered 20 min before the treatment of pilocarpine. Mice of Sham group were injected with saline solution. Only mice that displayed 90 min of SE survived and showed the following levels of seizure were selected: falling, wild running or jumping, clonic seizures, tonic–clonic seizures. To terminate the

SE, diazepam (15 mg/kg, i.p.; Sigma-Aldrich) was administered 90 min after onset.

Electrode installation

The mice were anesthetized with 1.25% 2,2,2-tribromoethanol (Avertin; 0.02 ml/g i.p.; Sigma-Aldrich) and mounted in a stereotaxic instrument (RWD Life Science Co., Ltd.). Three holes were drilled in the skull to allow the installation of three metal electrodes. The recording electrode was positioned above the right hippocampus (ML: 1.5 mm, AP: 2.0 mm). The reference electrode was situated on the opposite frontal bone, while the ground electrode was placed on the opposite occipital bone. All electrodes were fixed to the skull using dental cement with cyanoacrylate glue. After surgery, mice were kept in individual cages with food and water ad libitum.

EEG recordings and analysis

The mice were allowed to recover for 1 week from surgery. The electrodes were connected to an electroencephalogram (EEG) recorder (Beijing Solar Electronic Technologies Co., Ltd.). EEG data were recorded for 30 min as the baseline before lithium chloride injection. Then continuous recordings were performed from before pilocarpine treatment until the termination of SE.

The EEG acquisition software is equipped with features to automatically eliminate power frequency interference and conduct filtering. MATLAB R2023a was used for the processing and analysis of the EEG signal. For each data set, time–frequency analysis was conducted, and the power of the EEG signal was calculated in particular frequencies: total EEG band (0–100 Hz), delta (0.5–4 Hz), theta (4–8 Hz), alpha (8–12 Hz), beta (12–30 Hz), and gamma (30–70 Hz). Considering the variability in power values among mice, all data are standardized and presented as relative power, calculated as: (power/baseline power)−1.

MRI acquisition

MRI scanning was conducted on a horizontal 7.0 T scanner (PharmaScan 70/16 US, Bruker BioSpin), 30 min after SE onset or saline injection. Mice were anesthetized with inhaled isoflurane (3.0% for induction, 1.5% for maintenance) and positioned on a bed with mouth and ear bars to immobilize them during the experiments. Body temperature was controlled via regulated water flow and breathing rate was continuously monitored. Prior to diffusion-weighted imaging (DWI), all necessary adjustments and T2-weighted scans were performed to visualize the geometry, with parameters: repetition time/echo time (TR/TE) = 4200/52 ms, matrix = 256 × 256, field of view (FOV) = 25.6 × 25.6 mm^2, slice thickness = 0.7 mm. As previously described [21], diffusion-weighted images were obtained using a single-shot echo-planar encoding sequence with following parameters: TR/TE = 1325 / 63 ms, matrix = 128 × 128, FOV = 25.6 × 25.6 mm^2, slice thickness = 1 mm. Five images were acquired with different gradient gains, resulting in multiple b values (0, 400, 800, 1200, and 1600 s/mm^2). Apparent diffusion coefficient (ADC) images were generated from DWI scans using Paravision v.6.0.1 software (Bruker), and regions of interest (ROIs) were traced for the cortex on brain slices (bregma 1.0 to −2.5 mm). ADC values were then calculated and averaged.

Cortical water content measurement

Thirty minutes following SE onset or saline injection, mice were anesthetized and their brains were extracted, cortex were dissected and weighed, then dried in an oven at 100 °C for 24 h before being weighed again. The percentage of water content was calculated as: (wet weight-dry weight)/wet weight × 100%.

Sodium fluorescein penetration assay

To assess the BBB permeability during the initial 30 min following SE onset, mice were administered sodium fluorescein (NaFl; 10 mg/kg, i.p.; Sigma-Aldrich) at the time of onset (or 30 min after saline injection). Thirty minutes post-NaFl injection, mice were anesthetized, blood was collected via cardiac puncture. Plasma was extracted by centrifugation, mixed with an equal volume of 30% trichloroacetic acid and centrifuged again to extract NaFl. Following cardiac perfusion with phosphate-buffered saline (PBS), brains were harvested and homogenized with 30% trichloroacetic acid (150 µl/100 mg) using a tissue grinder (SWE-3D, Servicebio). The homogenate was then centrifuged to extract NaFl. A fluorescence microplate reader (Feyond-A300, Allsheng Instrument) quantified the NaFl fluorescence (excitation 470 nm, emission 520 nm). The NaFl permeability ratio in brain tissue was determined by calculating the ratio of brain tissue fluorescence to plasma fluorescence.

To visualize fluorescence penetration in brain slices, after transcardial perfusion with PBS, the brains were fixed in 4% paraformaldehyde (PFA) overnight, followed by cryoprotected in 30% sucrose solution for 2 days before being embedded in OCT. Then brains were sectioned into 100 µm thick slices using a cryostat. Six slices from each brain were collected (at 500 µm intervals, bregma + 0.50 mm to −2.5 mm), rinsed with PBS, and mounted on slides. Images of the slices were captured using a confocal microscope (Nikon AX). Fiji software (ImageJ 1.54f, National Institutes of Health, USA, available from https://fiji.sc/) was used to quantify the fluorescence intensity of the images, and the values for each brain were averaged.

Cisterna magna cannulation and head plate installation

Cisterna magna (CM) cannulation and head plate installation were performed as previously described [22]. Briefly, mice were anesthetized and placed in a stereotaxic frame, and the skin was removed to expose the frontal and parietal bones, as well as the cervical muscles. After rinsing the skull with sterile saline, a thin layer of clear-drying cyanoacrylate glue was applied. The cervical muscles were retracted to expose the CM, and a broken-tipped 30 G needle connected to a PE10 tube was inserted. Glue was applied, followed by a mixture of dental cement and glue to cover the skull and needle. Once the CM cannula was in place, drugs could be administered via the cannula. Next, the head plate was positioned on the parietal bone, aligning the observation window with the skull, and fixed using the dental cement mixture, which also covered the CM cannula. Following surgery, the mice either received transcranial imaging or were single-housed with food and water ad libitum. Daily 1-h adaptive training sessions with mice fixed in a head holder for 7 days prevented agitation during subsequent awake-state transcranial imaging.

Transcranial imaging

Mice were fixed in a head holder either awake or anesthetized and placed on the stage of the macroscope. Using a syringe pump, 10 μl of Alexa 555-conjugated ovalbumin (OVA, 45 kDa; 1 mg/ml diluted in artificial CSF; Invitrogen, O34782) was injected through the CM cannula at a rate of 2.5 μl/min. Tracer infusion and imaging were performed simultaneously, with images acquired every minute on the cy3 channel for 30 min. Each image was analyzed using FIJI software to quantify the percentage of tracer influx area in the bilateral cortex (region of interest, ROI) relative to the total area. Following image acquisition, the animals were decapitated, and brains were removed and fixed overnight in 4% PFA. For each mouse, six thick slices (100 μm) were cut, stained with DAPI, mounted, and imaged using a confocal microscope (Nikon AX). All 6 images were quantified as the percentage of signal area relative to the total slice area, and the average was calculated to obtain one value per mouse.

Depletion of PBMs

Mice were placed in a stereotaxic frame following anesthesia with Avertin. The neck skin was incised and muscles were retracted to expose the CM. A 33-gauge Hamilton syringe was employed for the injection. To prevent backflow, the syringe remained in place for 5 min post-injection before suturing the skin. To deplete PBMs, mice received an intra-cisterna magna (i.c.m.) injection of clodronate (CLO) liposomes (5 μl; YeaSen Biotechnology), while the control group received an i.c.m. injection of PBS liposomes (5 μl; YeaSen Biotechnology). Follow-up experiments were conducted 7 days after the treatment. In some experiments, drugs were administered through the cannula after CM cannulation was completed.

CSF drainage

Seven days post-cisterna magna catheterization, SE modeling commenced. Upon onset of SE seizures, a Hamilton syringe with an extension tube was attached to the catheter, and 15 μl of CSF was slowly extracted at 2.5 μl/min. Sham group mice underwent catheterization only, without CSF drainage.

Immunohistochemistry, imaging and quantification

After anesthesia with Avertin, mice were transcardially perfused with PBS followed by 4% PFA. In some experiments, mice were treated with lectin (30 μl; i.v.; Dylight 649 labelled Lycopersicon Esculentum; Invitrogen, L32472) 5 min prior to perfusion. Brains were removed and fixed in 4% PFA overnight, followed by cryoprotected in 30% sucrose solution for 2 days. For staining of CD206, brains were sectioned into 100-μm-thick slices, while others were cut into 30-μm-thick sections. Brain slices were rinsed in PBS and incubated with blocking solution (PBS containing 5% bovine serum albumin (BSA) and 0.3% Triton X-100) for 1 h at room temperature. After blocking, sections were incubated overnight at 4 °C with primary antibodies diluted in PBS containing 1% BSA and 0.3% Triton X-100: rat anti-CD206 (Invitrogen, MA5-1687; 1:500), rabbit anti-AQP4 (Proteintech, 16473-1-AP; 1:200), rabbit anti-Iba-1 (Wako, 019–19741; 1:1000), mouse anti-GFAP (Invitrogen, GA5; 1:500), rabbit anti-NeuN (Abcam, ab177487; 1:500), FITC-conjugated anti-mouse IgG (Sigma-Aldrich, F5262; 1:200). Following incubation, sections were washed in PBS and incubated for 2 h at room temperature with Alexa Fluor conjugated secondary antibodies (Invitrogen, A-11001/A-21209/A-21244; 1:1000), diluted in PBS containing 1% BSA and 0.3% Triton X-100. Tissue was washed in PBS after incubating with DAPI (Beyotime, C1006) for 10 min at room temperature and then mounted. According to the reagent instructions, Fluoro-Jade-C (FJC) staining (Biosensis, TR-100-FJT) was performed to assess neuronal injury. Images were acquired by confocal microscopy (Nikon AX). Quantitative analysis was conducted using FIJI software.

AQP4 polarization was defined as the ratio between the AQP4 intensity along the PVS area and global parenchymal domains [23, 24].

Statistical analyses

Statistical analysis was performed using GraphPad Prism 9 software. Data are presented as mean ± standard error of the mean (SEM). Unpaired t-test was used to determine statistical significance between two groups. Continuous data were analyzed by two-way ANOVA with Bonferroni's multiple comparison test. All tests were two-tailed, and a P value of < 0.05 was considered statistically significant ($^{*}P < 0.05$, $^{**}P < 0.01$, $^{***}P < 0.001$ and $^{****}P < 0.0001$).

Results

Cytotoxic edema formation in the initial phase of SE

Lithium chloride-pilocarpine was employed to induce SE in mice while concurrently recording EEG (Fig. 1A). Following seizure onset, EEG amplitude rapidly increased, after a few minutes of suppression, it rose again and maintained a high-amplitude pattern (Fig. 1B). Time–frequency analysis revealed that during SE, except for a few minutes of suppression after onset, power across all frequency bands was elevated, with the highest energy distributed within 50 Hz (Fig. 1C). Analysis of relative power at 10-min intervals showed a rapid increase in the first 30 min post-seizure onset, followed by divergence—leveling off (delta, theta) or rising then falling (total, alpha, beta, gamma) (Fig. 1D–I). The rapid relative EEG power increase reflected abnormal brain electrical activity intensification, indicating high energy demand during this phase. However, the brain often experiences hypoxic conditions during this period [25–27]. This significant imbalance leads to cerebral hypoxia and disrupted adenosine triphosphate (ATP) production. Na^+/K^+-ATPase dysfunction has been confirmed in humans and animal epilepsy studies [28]. This relates to elevated extracellular glutamate and K^+ concentrations, promoting seizures and cellular swelling [8, 29]. SE was traditionally defined as seizures lasting 30 min or longer, as this duration typically results in irreversible neuronal injury. Based on this definition, in this study we refer to the first 30 min of SE as the initial stage of SE [1, 2]. We utilized ADC maps from DWI for measurement and found that in the initial of SE, ADC values of bilateral cortex were significantly lower compared in SE versus sham mice (Fig. 1J–L). Simultaneously, cortical water content was higher in SE mice (Fig. 1M), suggesting the development of cytotoxic edema and altered tissue fluid volume during the initial phase of SE.

CSF is an important fluid source for cerebral edema during the initial phase of SE

Traditionally, it was thought that cytotoxic edema stage solely involved the movement of interstitial fluid into cells, without additional fluid accumulation, and net fluid increase only occurred during ionic edema or after BBB disruption [30]. However, our experiments revealed that in the mouse cortex, cytotoxic edema coincided with increased brain water content during early SE, and the marked decrease in ADC values did not support the inference that the mice were experiencing vasogenic edema [4, 31]. Drawing from recent studies on ischemic stroke and anoxic cerebral edema [9, 10], we suspected that CSF might contribute to the development of cerebral edema during the initial phase of SE. To examine early BBB permeability and blood fluid influx in early SE, we utilized NaFl (Fig. 2A), a small molecular weight (376 Da) hydrophilic molecule, which is regarded as a sensitive marker of BBB early disruption [32–37]. By quantifying the fluorescence intensity of NaFl, we found no substantial increase in the quantity of NaFl infiltrating from the blood into the brain within 30 min of SE onset (Fig. 2D), and no significant increase in fluorescence intensity was detected in the visualized brain slices (Fig. 2B, C). Subsequently, to investigate CSF transport at this stage, we utilized transcranial imaging and observed that, under awake conditions, within 30 min after the onset, there was a significant increase in the influx of CSF tracer in the bilateral cerebral cortex (Fig. 2E-H). Quantitative analysis of fluorescent tracer in brain slices also showed higher tracer amounts in SE mice (Fig. 2I, J). As blood flow persists during SE, fluid contribution from the blood cannot be completely ruled out. Nevertheless, the aforementioned data indicate that CSF is an important fluid source during the initial stage of SE.

CSF influx significantly reduces following PBM depletion

Recent studies on PBMs [20] led us to hypothesize that they may affect CSF flow into the cortex and contribute to cerebral edema following SE. To deplete PBMs, mice received CLO liposome administration via i.c.m. injection. Seven days post-depletion, we observed a significant reduction in PBM coverage (Fig. 3A-C). Transcranial imaging assessed CSF transport and distribution in PBM-depleted mice, revealing a marked decrease in fluorescent tracer flow into the cortex (Fig. 3D–G). Quantitative analysis of brain slices also showed significantly lower OVA coverage (Fig. 3H, I). Situated on the endfeet of perivascular astrocytes, AQP4 plays a crucial role in regulating CSF circulation [38, 39]. To determine if PBM depletion impacts AQP4, we conducted immunohistochemical (IHC) detection. However, no significant alterations in AQP4 coverage or polarization index were observed following PBM depletion (Fig. 3J–L). These findings indicate that the decreased CSF influx resulting from PBM depletion occurs independently of AQP4, consistent with prior research outcomes [20].

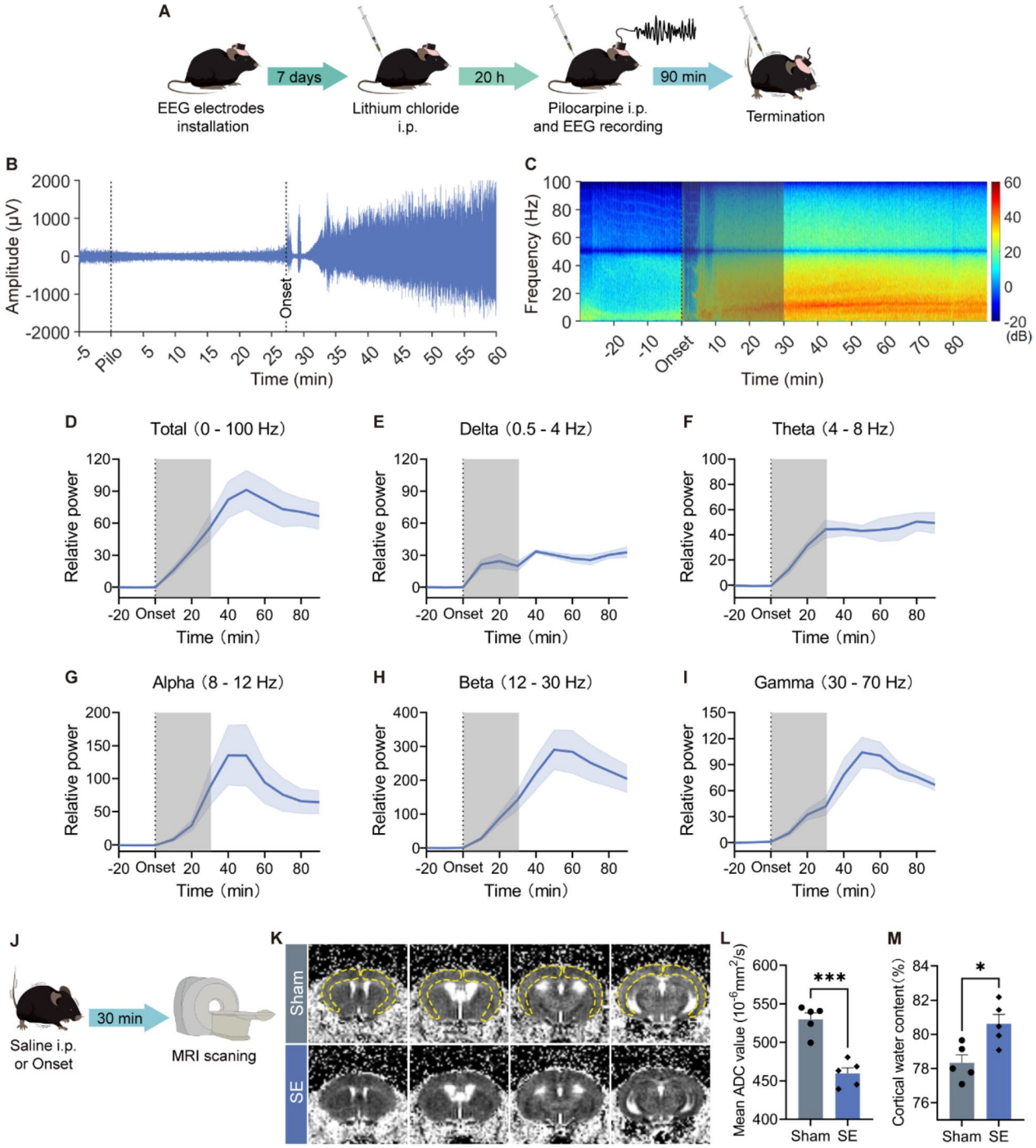

Fig. 1 Relative EEG power increased and ADC value decreased during the initial phase of SE. **A** Schematic of experiment. **B** Representative EEG tracings in mice treated with pilocarpine. **C** Representative time–frequency power distribution diagram pre- and post-onset of SE. The gray rectangles represent the initial stage of SE. **D**–**I** Changes in relative power of various frequency bands pre- and post-onset of SE. The gray rectangle represents the initial stage of SE. n = 5. **J** Schematic of experiment. **K** Representative ADC images reconstructed after DWI scans. The ROIs indicate the calculation regions for bilateral cortical ADC values. **L** Quantification of mean ADC values of the bilateral cortex. n = 5 per group. **M** Quantification of cortical water content. n = 5 per group. Data are presented as mean ± SEM, unpaired t-test. *P < 0.05, ***P < 0.001

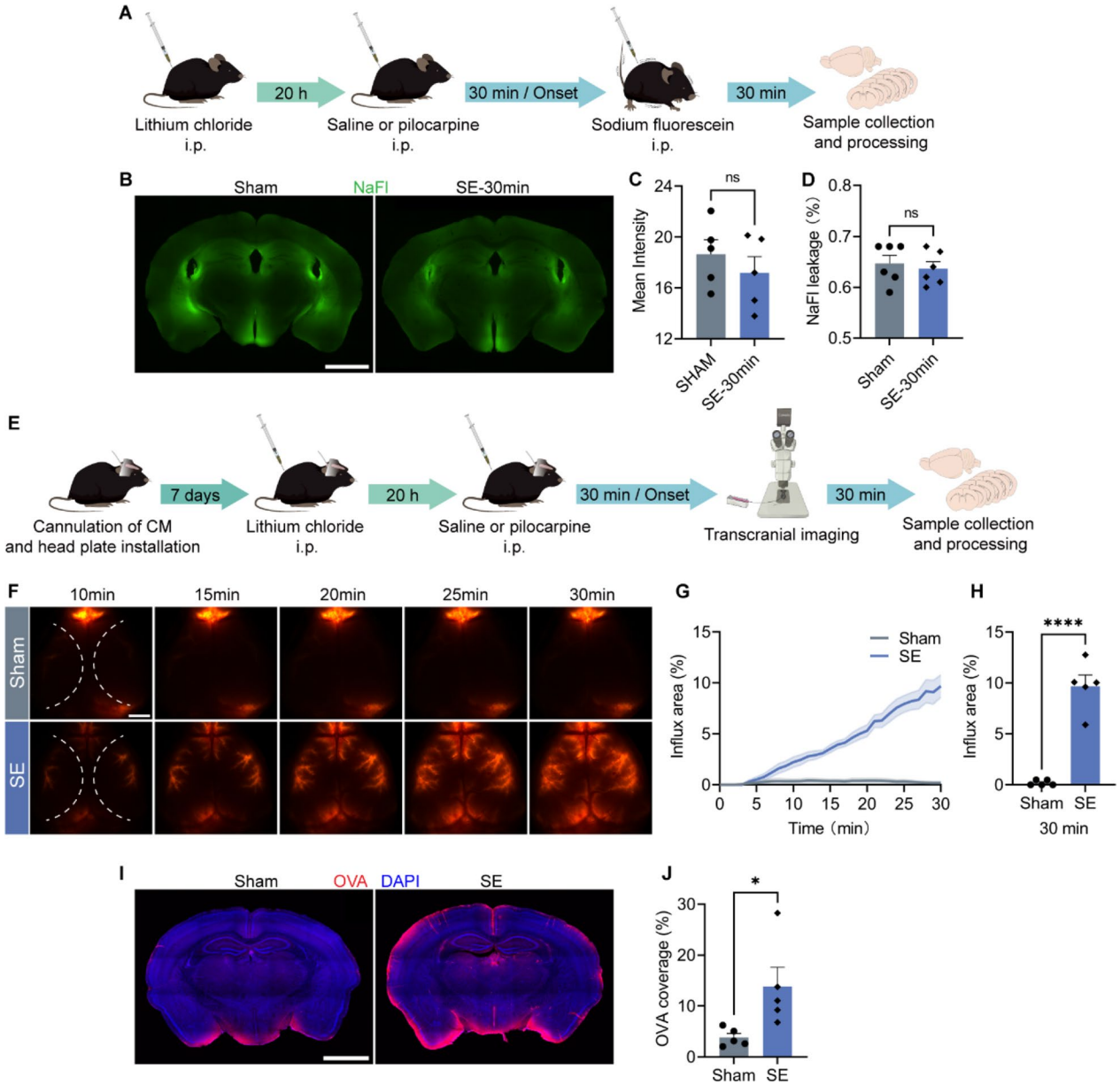

Fig. 2 CSF is an important source of cerebral edema during the initial stage of SE. **A** Schematic of experiment. **B** Representative images of visualized NaFl leakage. Scale bar = 2 mm. **C** Quantification of the mean fluorescence intensity of NaFl in brain sections. n = 5 per group. **D** Quantification of the proportion of NaFl leakage into brain tissue. n = 6 per group. **E** Schematic of experiment. **F** Representative images of fluorescent tracer transport and distribution within 30 min after CM injection. Scale bar = 2 mm. The dashed area represents the ROIs included in the quantification. **G** Influx area of fluorescent tracer during the 30 min after CM injection, quantified from the ROIs in (**F**). n = 5 per group. **H** Quantification of the influx area of fluorescent tracer at 30 min. n = 5 per group. **I** Representative images of fluorescent tracer coverage in brain sections. Scale bar = 2 mm. **J** Quantification of the fluorescent tracer coverage. n = 5 per group. Data are presented as mean ± SEM, unpaired t-test. *P < 0.05, ****P < 0.0001, ns = not significant

PBM depletion has no effect on SE susceptibility and EEG power

To investigate whether PBM depletion affects SE in mice, we performed SE modeling and collected EEG data after depletion (Fig. 4A, B). Time–frequency analysis showed that during SE, apart from a brief suppression period following onset, EEG power across all frequency bands was significantly elevated in both groups of mice, with highest energy distributed within 50 Hz (Fig. 4C). The relative power of each band over time was analyzed at 10-min intervals for both groups, and inter-group differences were assessed using two-way ANOVA with

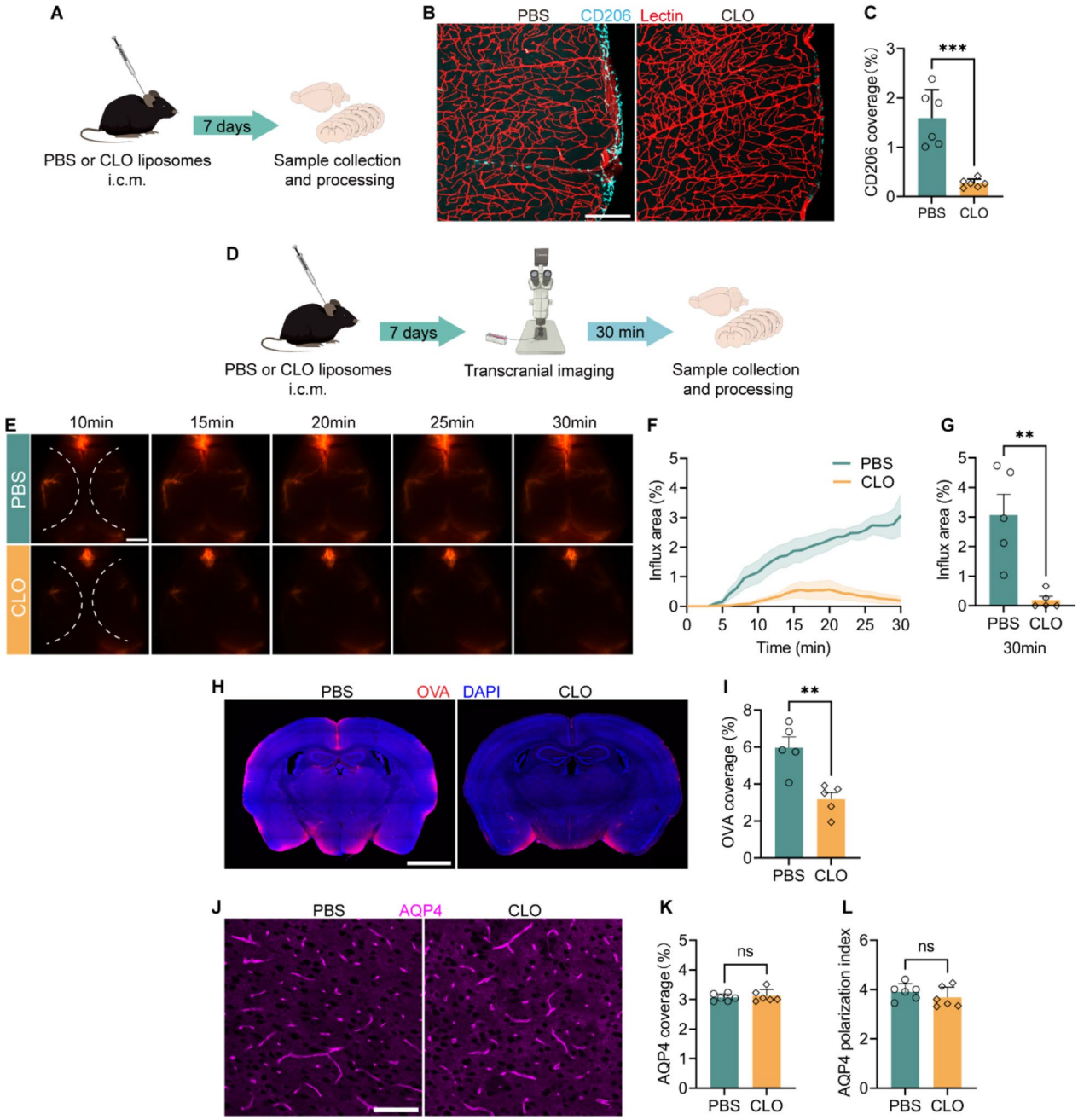

Fig. 3 CSF influx decreases after depletion of PBM. **A** Schematic of experiment. **B** Representative images of brain sections showing CD206 and lectin staining. Scale bar = 200 μm. **C** Quantification of the coverage of $CD206^{+}$ cells. n = 6 per group. **D** Schematic of experiment. **E** Representative images of fluorescent tracer distribution within 30 min after CM injection. Scale bar = 2 mm. The dashed area represents the ROIs included in the quantification. **F** Influx area of fluorescent tracer during the 30 min after CM injection, quantified from the ROIs in (**E**). n = 5 per group. **G** Quantification of the influx area of fluorescent tracer at 30 min. n = 5 per group. **H** Representative images of fluorescent tracer coverage in brain sections. Scale bar = 2 mm. **I** Quantification of the fluorescent tracer coverage. n = 5 per group. **J** Representative images of AQP4 expression in the cerebral cortex. Scale bar = 100 μm. **K** Quantification of AQP4 coverage. **L** Quantification of the polarization index of AQP4. For **K** and **L**. n = 6 per group. Data are presented as mean ± SEM, unpaired t-test. $^{**}P < 0.01$, $^{***}P < 0.001$, ns = not significant

Bonferroni's multiple comparison correction. The results showed no significant changes in the relative EEG power in CLO-treated mice across all bands: total ($p = 0.8800$), delta ($p = 0.4400$), theta ($p = 0.6378$), alpha ($p = 0.7650$), beta ($p = 0.3652$), and gamma ($p = 0.2749$). The time × treatment interaction was also not significant

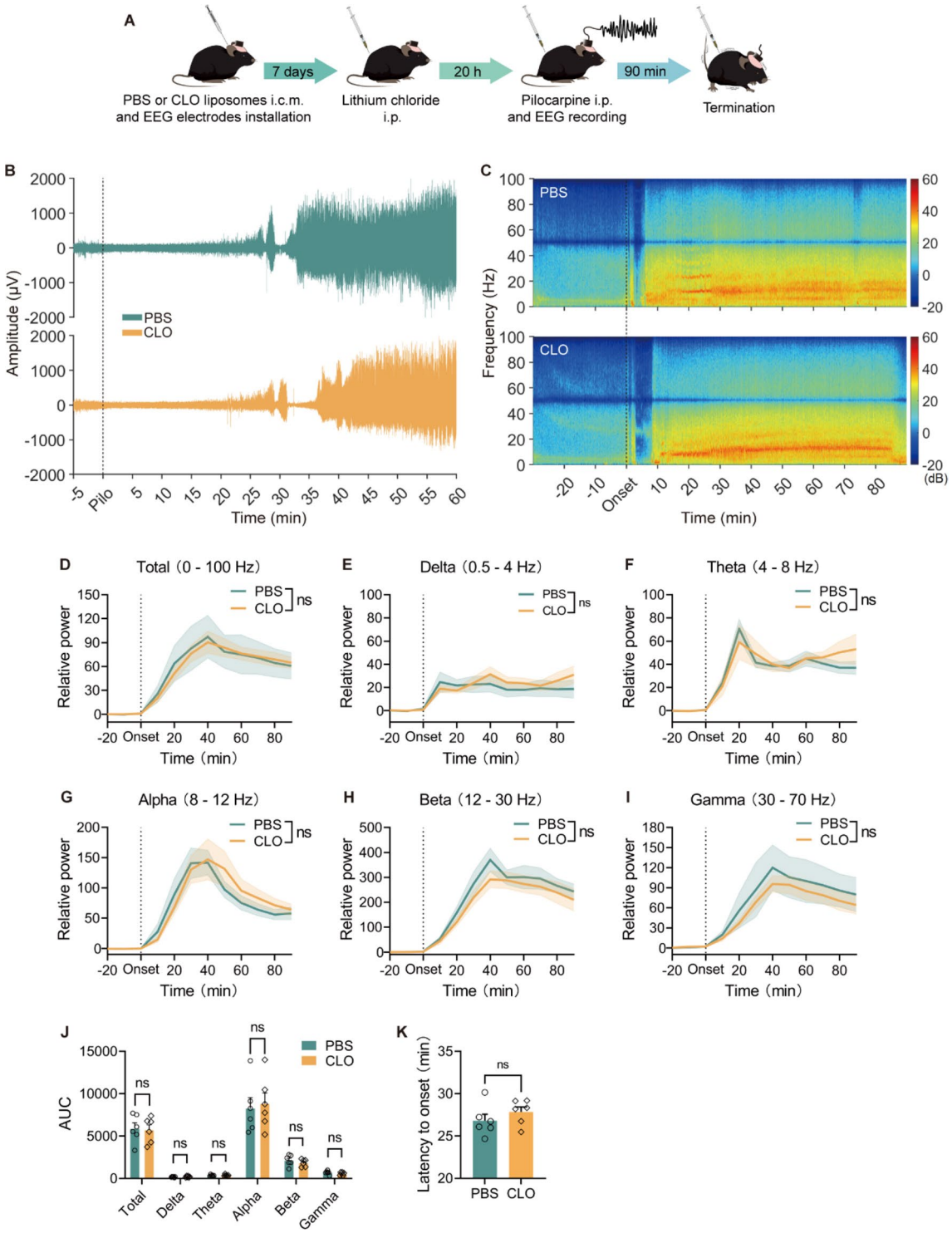

Fig. 4 PBM depletion does not impact SE susceptibility and EEG power. **A** Schematic of experiment. **B** Representative EEG tracings in mice treated with pilocarpine. **C** Representative time–frequency power distribution diagram pre- and post-onset. **D**–**I** Quantitative analysis of the relative EEG power pre- and post-onset. Data are presented as mean ± SEM. Differences among multiple groups were examined by two-way ANOVA with Bonferroni's multiple comparison test. n = 6 per group. **J** Quantification of the AUC in (**D**–**I**) for the PBS and CLO group. **K** Quantitative analysis of the latency period for the onset. For **J** and **K**, n = 6 per group. Data are presented as mean ± SEM, unpaired t-test. ns = not significant

for all bands: total ($p=0.9418$), delta ($p=0.0863$), theta ($p=0.6586$), alpha ($p=0.5872$), beta ($p=0.8964$), and gamma ($p=0.8136$) (Fig. 4D, I). Furthermore, there were no significant differences in the area under the curve (AUC) of the relative power between groups for each band (Fig. 4J). Using the latency to onset as an indicator of susceptibility, mice with PBM depletion did not exhibit significant shortening or prolongation (Fig. 4K). These data suggest PBM depletion does not exert a direct positive or negative impact on SE in mice.

PBM depletion alleviates cerebral edema following SE

In the above experiments, we observed that during initial SE, CSF influx increased and cytotoxic edema formed. Interestingly, this influx was significantly reduced following PBM depletion. To further investigate the role of this treatment in SE-induced cerebral edema, we performed SE modeling 7 days after CLO or PBS liposomes injection (Fig. 5A). Transcranial imaging revealed markedly decreased tracer influx in PBM-depleted mice within 30 min post-onset, confirmed by brain section analysis showing significantly lower OVA coverage (Fig. 5B–F). Cortical water content was also lower in PBM-depleted mice compared to controls (Fig. 5G). Additionally, DWI scans 30 min post-onset showed higher ADC values in PBM-depleted mice (Fig. 5H–J), indicating a milder degree of cytotoxic edema. Cytotoxic edema is a critical initiating step driving cerebral edema development, closely associated with subsequent ionic and vasogenic edema. Vasogenic edema reaches its peak on days 2–3 following SE, coinciding with the greatest accumulation of IgG leakage from blood vessels into the brain parenchyma [3, 40–42]. IHC performed on day 3 post-SE showed significantly reduced IgG leakage in PBM-depleted mice (Fig. 5K, L), consistent with their lower cortical water content (Fig. 5M). To explore whether this reduction in edema was directly related to CSF flow, we performed cisterna magna cannulation to drain CSF at SE onset (Fig. S1A). This intervention resulted in reduced IgG leakage and lower cortical water content 3 days post-SE (Fig. S1B-D), suggesting attenuated vasogenic edema. Collectively, these findings indicate PBM depletion alleviates both cytotoxic and vasogenic edema following SE.

Depletion of PBM alleviates neuroinflammation and neuronal injury induced by SE

Cerebral edema not only results from neuroinflammation but also triggers or exacerbates secondary injury and inflammatory responses [5, 6]. During the inflammatory process, microglia and astrocytes are activated, leading to the release of pro-inflammatory factors and neurotoxic effects [43]. Previous studies have demonstrated that following pilocarpine-induced SE, microglia rapidly activate and proliferate, while astrocyte numbers decrease within 3 days post-SE, displaying abnormal morphology. However, after 10 days, astrocyte numbers recover, and the cells proliferate and exhibit hypertrophy [44, 45]. We then investigated whether depleting PBMs mitigates neuroinflammation and neuronal injury following SE. Before SE modeling, we assessed Iba-1 and GFAP immunoreactivity in cortex and hippocampus, finding no significant changes after CLO treatment, suggesting that PBM depletion does not directly influence microglial and astrocytic expression under physiological conditions. We then conducted tests on days 1, 3, and 7 post-SE. Iba-1^+ cells displayed activated morphology on all 3 days, but their numbers were lower in the cortex and hippocampus of PBM-depleted mice (Fig. 6A–C). $GFAP^+$ cells showed no significant differences in the cortex and hippocampus on day 1 post-SE and exhibited atrophied morphology. On day 3 post-SE, $GFAP^+$ cell numbers were lower in cortex of PBM-depleted mice but not hippocampus. By day 7 post-SE, proliferating and hypertrophic $GFAP^+$ cells were observed in all mice, albeit with lower numbers in cortex and hippocampus of PBM-depleted mice (Fig. 6A, B, D). To examine whether these changes were related to CSF inflow, we conducted experiments on CSF-drained mice and control mice. We found that 3 days after SE, CSF-drained mice exhibited reduced Iba-1^+ cells in both cortex and hippocampus, and decreased $GFAP^+$ cells in the cortex (Fig. S2A-D). Furthermore, we assessed NeuN reactivity in cortex and hippocampus of non-SE mice, finding no significant changes in CLO-treated mice (Fig. 7A, B). Lastly, we employed FJC staining to evaluate hippocampal neuronal damage on day 7 post-SE, revealing significantly fewer FJC^+ cells in the hippocampus of PBM-depleted mice (Fig. 7C, D). These findings indicate that PBM depletion attenuates both neuroinflammation and neuronal injury induced by SE.

Discussion

Cerebral edema is an inevitable complication of various CNS disorders and may be fatal in severe cases. Prior studies on cerebral edema following SE have primarily concentrated on the phase of BBB disruption, while the earlier stages have received minimal attention. In the present study, we discovered that CSF influx contributes to cerebral edema development during the initial phase of SE. Depletion of PBM diminished CSF inflow, mitigated cytotoxic edema in the early stage of SE and subsequent vasogenic edema, as well as attenuating the inflammatory response and neuronal injury post-SE.

The conventional wisdom is that cerebral edema fluid is exclusively derived from blood [8]. However, recent studies have updated our understanding of edema formation mechanism. Cytotoxic edema occurs after stroke

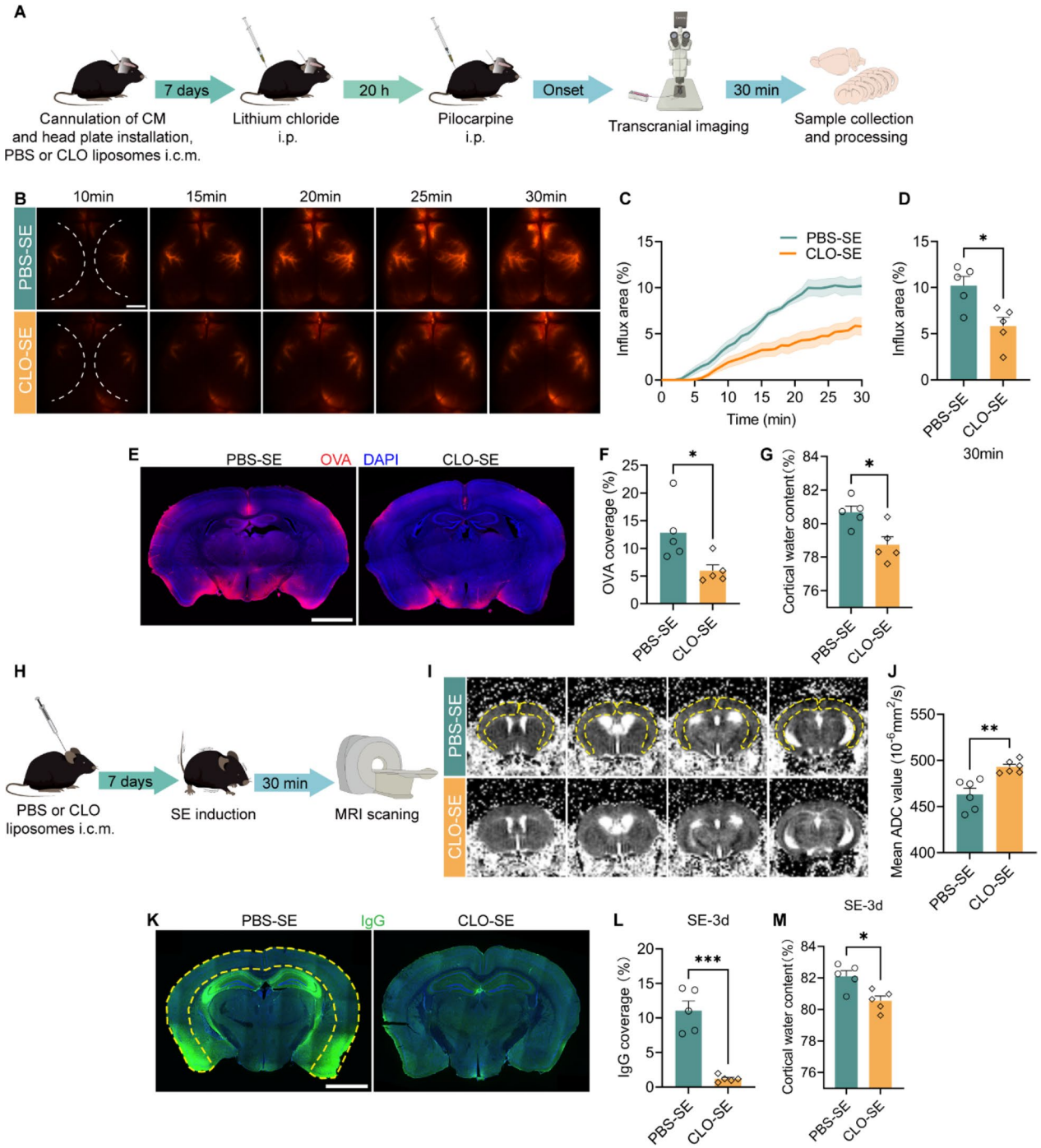

Fig. 5 PBM depletion attenuates cerebral edema following SE. **A** Schematic of experiment. **B** Representative images of fluorescent tracer distribution within 30 min after CM injection. Scale bar = 2 mm. The dashed area represents the ROIs in the bilateral cortex included in the quantification. **C** Influx area of fluorescent tracer during the 30 min after CM injection, quantified from the ROIs in (**B**). n = 5 per group. **D** Quantification of the influx area of fluorescent tracer at 30 min. n = 5 per group. **E** Representative images of fluorescent tracer coverage in brain sections. Scale bar = 2 mm. **F** Quantification of the fluorescent tracer coverage. n = 5 per group. **G** Quantification of cortical water content. n = 5 per group. **H** Schematic of experiment. **I** Representative ADC images reconstructed after DWI scans. **J** Quantification of mean ADC values of the bilateral cortex. n = 5 per group. **K** Representative images of IgG leakage in brain parenchyma. Scale bar = 2 mm. **L** Quantitative analysis of IgG leakage. n = 5 per group. **M** Quantification of cortical water content. n = 5 per group. Data are presented as mean ± SEM, unpaired t-test. *P < 0.05, **P < 0.01, ***P < 0.001

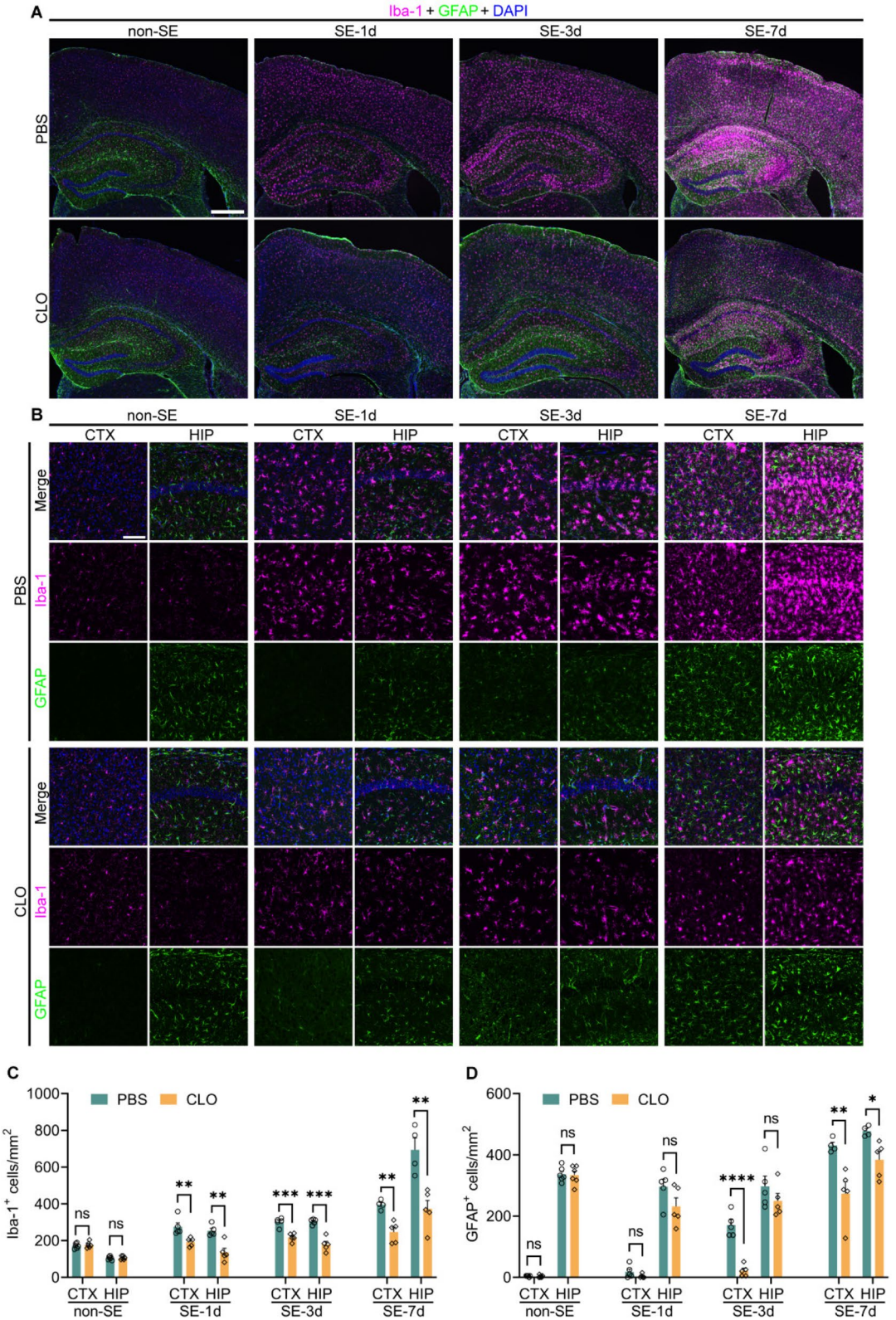

Fig. 6 PBM depletion alleviates neuroinflammation following SE. **A** Panoramic stitched images of Iba-1$^+$ cells and GFAP$^+$ cells in cortex and hippocampal region. 10 × magnification field of view. Scale bar = 500 μm. **B** Representative images of Iba-1$^+$ cells and GFAP$^+$ cells in cortex and hippocampal region. 40 × magnification field of view. Scale bar = 100 μm. **C**, **D** Quantification of Iba-1$^+$ cells and GFAP$^+$ cells. n = 4–6 per group. Data are presented as mean ± SEM, unpaired t-test. *P < 0.05, **P < 0.01, ***P < 0.001, ****P < 0.0001, ns = not significant

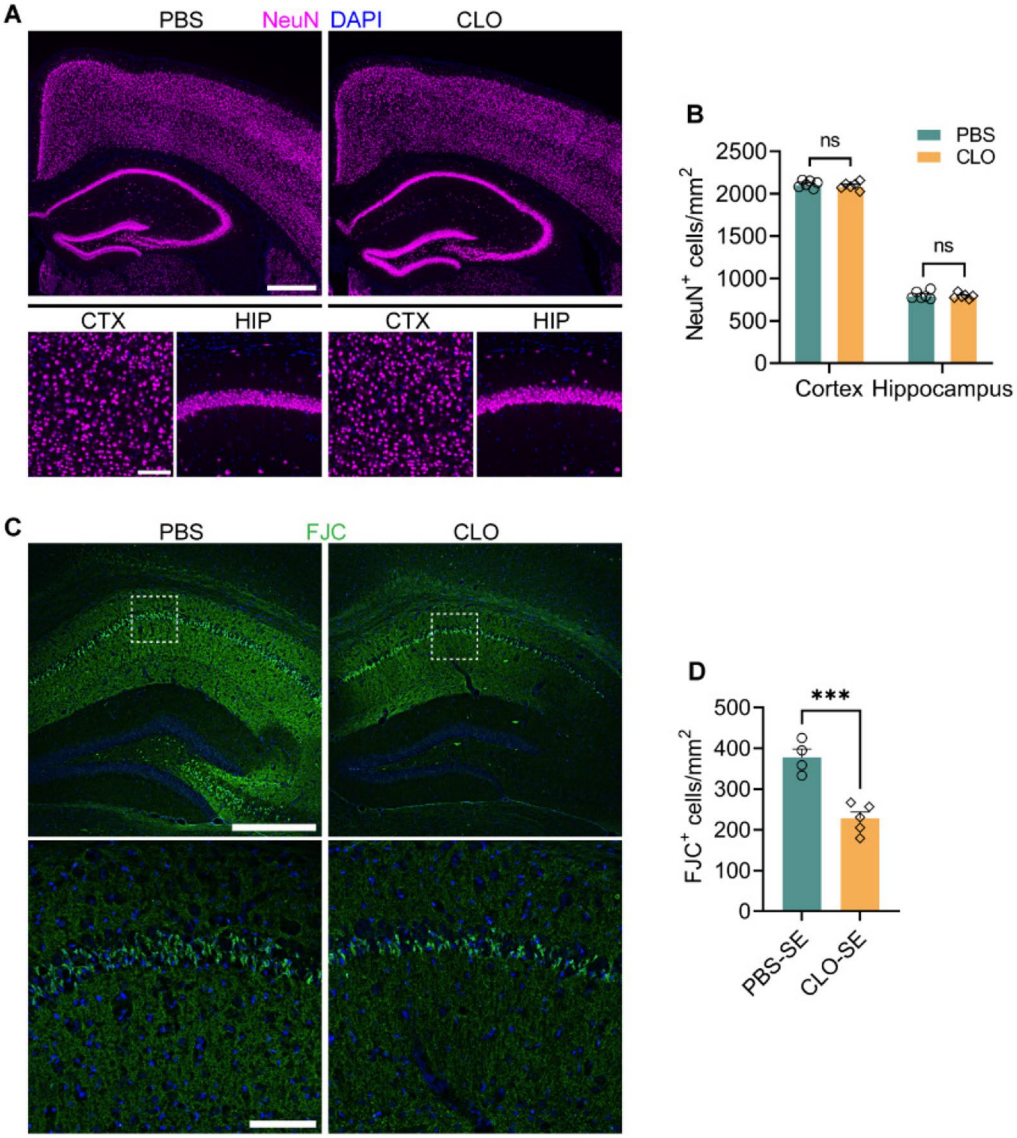

Fig. 7 PBM depletion attenuates neuronal injury induced by SE. **A** Representative images of NeuN$^+$ cells in cortex and hippocampal region. 10 × magnification field of view; scale bar = 500 μm (the top images). 40 × magnification field of view; scale bar = 100 μm (the bottom images). **B** Quantification of NeuN$^+$ cells. n = 6 per group. **C** Representative images of FJC staining in the hippocampal region. 10 × magnification field of view; scale bar = 500 μm (the top images). 40 × magnification field of view; scale bar = 100 μm (the bottom images). **D** Quantification of FJC$^+$ cells. n = 4–5 per group. Data are presented as mean ± SEM, unpaired t-test, ***P < 0.001, ns = not significant

and cardiac arrest, where rapid CSF influx in the complete absence of blood flow provides Na^+ and water to ischemic tissues. In this process, high osmotic gradients and spreading depolarization-induced intense arteriolar constriction provide the driving forces for rapid CSF influx. The arteriolar constriction causes the perivascular space (PVS) to suddenly expand and its pressure to reduce, sucking fluid into tissues [9, 10]. In this study, excessive neuronal firing and synchronized discharges were observed within 30 min of seizure onset, i.e., the initial phase, as EEG power rapidly increased, indicating the brain urgently required more energy. However, vascular spasms and hypoperfusion predominated at this stage [26, 46, 47]. While some reported congestion and increased perfusion during seizures [48, 49], quantitative modeling found that when vasospasm occurs causing heterogeneous perfusion, increased cerebral blood flow actually exacerbates hypoxia [50]. Spasms drive extravascular fluid influx by altering pressure balances while intensifying severe mismatches between heightened

metabolism and compromised oxygen delivery, inducing hypoxia and halting ATP production. Abnormal Na^+/K^+-ATPase function closely associates with elevated extracellular glutamate and potassium, instigating seizures and cytotoxic edema, and novel ion gradients power subsequent ionic fluid surges [8, 28, 29]. ADC cannot distinguish between intracellular and extracellular diffusion restriction. We observed decreased ADC values during the initial stage of SE, indicating cytotoxic edema formation [4, 31], while increased brain water content suggested external fluid ingress [8]. While blood flow was not completely absent during SE, we did not observe BBB permeability changes or increased blood-derived fluid but rather increased CSF influx during initial SE stage, suggesting CSF contributes to edema formation.

It is worth noting that while we were preparing this manuscript, a study was reported that provided an alternative explanation for the possible mechanism of increased CSF influx during the early SE. Synchronized neuronal discharges during sleep generate large, rhythmic ionic waves in the ISF, which enhance CSF influx into the brain tissue and serve to remove metabolic wastes generated by neuronal activity. In contrast, during waking, neurons discharge highly desynchronized, cancelling out one another's field potentials in the ISF and resulting in only minor fluctuations and significantly reduced CSF influx [11]. Another study also found a strong correlation between neuronal activity (elevated delta and beta power) and CSF influx [51]. Similarly, during the initial stage of SE, massive synchronized high-amplitude neuronal firing led to rapid increases across frequency bands, accompanied by a significant rise in CSF influx. From this perspective, during SE neurons generate more metabolic waste, abnormal glutamate accumulation, and imbalances in ion gradients. The enhanced synchronous firing and activity promote greater CSF influx for flushing. However, under pathological conditions, this mechanism is unable to serve its beneficial physiological role and instead facilitates the development of cerebral edema.

PBMs originate from early erythroid progenitor cells within the yolk sac, localizing to the PVS and pia mater. While the roles of PBMs in neurological diseases are complex [14–19], their precise functions in epilepsy remain unclear. We observed reduced CSF influx following PBM depletion, a change that persisted in the initial SE stage. Although PBM-depleted mice exhibited no alteration in SE severity or susceptibility, cerebral cortical ADC values exceeded controls, indicating reduced CSF influx is associated with attenuated cytotoxic edema. Prior studies showed PBMs regulate matrix metalloproteinase (MMP) activity modulating the extracellular matrix (ECM) enclosing vessels, thereby impacting PVS and arterial stiffness to govern CSF flow [20]. Our findings elucidate PBM involvement in cerebral edema genesis. Additionally, data showed milder vasogenic edema in PBM-depleted mice, partly from attenuated cytotoxic edema as the primary driving edema force [8], and partly from ECM accumulation and BBB permeability decline following PBM depletion [17, 18, 20].

Cerebral edema and neuroinflammation can exacerbate each other through a vicious cycle [5, 6]. While short-term neuroinflammation is neuroprotective, prolonged neuroinflammation can lead to neural damage [52]. During the inflammatory response, microglia and astrocytes are activated and release inflammatory factors [43]. According to previous studies, microglia rapidly activate and proliferate after SE, whereas astrocytes first undergo degeneration before recovering, proliferating and hypertrophying [44, 45]. We observed a similar sequence of events. As with other research, depletion of PBM did not impact microglia and astrocytes under physiological conditions. However, PBM-depleted mice exhibited lower numbers of activated microglia following SE, and while astrocyte degeneration did not differ significantly, proliferation was reduced, suggesting a milder inflammatory response after SE. The degree of neural damage also reflected differences in neuroinflammation between the two groups, with PBM-depleted mice experiencing lighter neural injury post-SE. Although PBM depletion-induced immunosuppression remains a possibility, our CSF drainage experiments yielded similar results: decreased IgG leakage and attenuated inflammation. This indicates that alterations in CSF inflow contribute to these effects.

As previously mentioned, PBM plays a dual role in neurological disorders. Depletion of PBM impairs brain clearance in AD [20], highlighting the long-term effects of PBMs on CSF flow regulation. However, we observed positive effects of PBMs in short-term pathological processes such as cerebral edema. Further studies utilizing diverse methods are required to investigate the long-term impacts of PBMs following SE.

In addition, our study focused on the function of PBMs in regulating CSF flow dynamics. However, to more comprehensively explore the role of PBMs in epilepsy, future work needs to pay attention to the functions of PBMs as immune cells situated at the blood–brain border and brain-fluid boundary in inflammation, such as phagocytosis and antigen presentation [13, 53].

In summary, we show that CSF contributes to cerebral edema formation during SE, and PBM depletion attenuated cerebral edema and inflammatory responses post-SE. This study adds insight into the mechanisms behind cerebral edema development during SE and the role of PBMs therein, pointing to potential new therapeutic strategies.

Abbreviations

SE	Status epilepticus
CSF	Cerebrospinal fluid
ISF	Interstitial fluid
PBM	Parenchymal border macrophage
PVS	Perivascular spaces
BBB	Blood–brain barrier
EEG	Electroencephalogram
DWI	Diffusion-weighted imaging
ADC	Apparent diffusion coefficient
CLO	Clodronate
CM	Cisterna magna
NaFl	Sodium fluorescein

Supplementary Information

The online version contains supplementary material available at https://doi.org/10.1186/s12967-024-05912-2.

Supplementary material 1.

Acknowledgements
Not applicable.

Author contributions
R.Lin. and J.Z. designed the study. R.Lin., J.Z., and R.Luo. performed the experiments. X.H. contributed to this work with materials and methods. R.Lin., R.Luo., and X.Y. analyzed the data. R.Lin wrote the manuscript. J.Z. and Y.G. revised the manuscript. All authors read and approved the final manuscript.

Funding
This work was supported by National Natural Science Foundation of China (Grant NO.82071452, Grant NO.82271488).

Availability of data and materials
Raw data can be accessed upon request by contacting the corresponding author.

Declarations

Ethics approval and consent to participate
The experiments were approved by the Animal Ethics Committee of Zhujiang Hospital of Southern Medical University (Certificate number: LAEC-2023-050) and were performed according to the Guide for the Care and Use of Laboratory Animals published by the National Institutes of Health of the United States.

Consent for publication
Not applicable.

Competing interests
The authors declare no competing interests.

Author details
[1]The National Key Clinic Specialty, The Engineering Technology Research Center of Education Ministry of China, Guangdong Provincial Key Laboratory On Brain Function Repair and Regeneration, Department of Neurosurgery, Zhujiang Hospital, Southern Medical University, Guangzhou 510000, China. [2]Dermatology Hospital, Southern Medical University, Guangzhou 510000, China. [3]Dongguan University of Technology, Dongguan 510282, China.

Received: 12 August 2024 Accepted: 21 November 2024
Published online: 02 December 2024

References

1. Trinka E, Cock H, Hesdorffer D, Rossetti AO, Scheffer IE, Shinnar S, et al. A definition and classification of status epilepticus–report of the ilae task force on classification of status epilepticus. Epilepsia. 2015;56:1515–23.
2. Betjemann JP, Lowenstein DH. Status epilepticus in adults. The Lancet Neurology. 2015;14:615–24.
3. Itoh K, Inamine M, Oshima W, Kotani M, Chiba Y, Ueno M, et al. Prevention of status epilepticus-induced brain edema and neuronal cell loss by repeated treatment with high-dose levetiracetam. Brain Res. 2015;1608:225–34.
4. Mendes A, Sampaio L. Brain magnetic resonance in status epilepticus: a focused review. Seizure. 2016;38:63.
5. Stamatovic SM, Dimitrijevic OB, Keep RF, Andjelkovic AV. Inflammation and brain edema: new insights into the role of chemokines and their receptors. Acta Neurochir Suppl. 2006;96:444–50.
6. Huang Y, Chen S, Luo Y, Han Z. Crosstalk between Inflammation and the BBB in Stroke. Curr Neuropharmacol. 2020;18:1227–36.
7. Gorter JA, van Vliet EA, Aronica E. Status epilepticus, blood-brain barrier disruption, inflammation, and epileptogenesis. Epilepsy Behav E&B. 2015;49:13–6.
8. Stokum JA, Gerzanich V, Simard JM. Molecular pathophysiology of cerebral edema. J Cereb Blood Flow Metab. 2016;36:513–38.
9. Mestre H, Du T, Sweeney AM, Liu G, Samson AJ, Peng W, et al. Cerebrospinal fluid influx drives acute ischemic tissue swelling. Science. 2020;367:eaax7171.
10. Du T, Mestre H, Kress BT, Liu G, Sweeney AM, Samson AJ, et al. Cerebrospinal fluid is a significant fluid source for anoxic cerebral oedema. Brain. 2021;145:787–97.
11. Jiang-Xie L-F, Drieu A, Bhasiin K, Quintero D, Smirnov I, Kipnis J. Neuronal dynamics direct cerebrospinal fluid perfusion and brain clearance. Nature. 2024;627:157–64.
12. Mildenberger W, Stifter SA, Greter M. Diversity and function of brain-associated macrophages. Curr Opin Immunol. 2022;76:102181.
13. Kierdorf K, Masuda T, Jordão MJC, Prinz M. Macrophages at CNS interfaces: ontogeny and function in health and disease. Nat Rev Neurosci. 2019;20:547–62.
14. Polfliet MM, Zwijnenburg PJ, van Furth AM, van Poll T, Döpp EA, de Lavalette CR, et al. Meningeal and perivascular macrophages of the central nervous system play a protective role during bacterial meningitis. J Immunol. 2001;167:4644–50.
15. Michaud J-P, Bellavance M-A, Préfontaine P, Rivest S. Real-time in vivo imaging reveals the ability of monocytes to clear vascular amyloid beta. Cell Rep. 2013;5:646–53.
16. Thanopoulou K, Fragkouli A, Stylianopoulou F, Georgopoulos S. Scavenger receptor class B type I (SR-BI) regulates perivascular macrophages and modifies amyloid pathology in an Alzheimer mouse model. Proc Natl Acad Sci USA. 2010;107:20816–21.
17. Santisteban MM, Ahn SJ, Lane D, Faraco G, Garcia-Bonilla L, Racchumi G, et al. Endothelium-macrophage crosstalk mediates blood-brain barrier dysfunction in hypertension. Hypertension. 2020;76:795–807.
18. Pedragosa J, Salas-Perdomo A, Gallizioli M, Cugota R, Miró-Mur F, Briansó F, et al. CNS-border associated macrophages respond to acute ischemic stroke attracting granulocytes and promoting vascular leakage. Acta Neuropathol Commun. 2018;6:76.
19. Polfliet MMJ, van Veerdonk F, Döpp EA, van Kesteren-Hendrikx EML, van Rooijen N, Dijkstra CD, et al. The role of perivascular and meningeal macrophages in experimental allergic encephalomyelitis. J Neuroimmunol. 2002;122:1.
20. Drieu A, Du S, Storck SE, Rustenhoven J, Papadopoulos Z, Dykstra T, et al. Parenchymal border macrophages regulate the flow dynamics of the cerebrospinal fluid. Nature. 2022;611:585–93.
21. Bozza FA, Garteiser P, Oliveira MF, Doblas S, Cranford R, Saunders D, et al. Sepsis-associated encephalopathy: a magnetic resonance imaging and spectroscopy study. J Cereb Blood Flow Metab. 2010;30:440–8.
22. Sweeney AM, Plá V, Du T, Liu G, Sun Q, Peng S, et al. In vivo imaging of cerebrospinal fluid transport through the intact mouse skull using fluorescence macroscopy. 2019. J Vis Exp. https://doi.org/10.3791/59774-v.
23. Kress BT, Iliff JJ, Xia M, Wang M, Wei HS, Zeppenfeld D, et al. Impairment of paravascular clearance pathways in the aging brain. Ann Neurol. 2014;76:845–61.

24. Si X, Dai S, Fang Y, Tang J, Wang Z, Li Y, et al. Matrix metalloproteinase-9 inhibition prevents aquaporin-4 depolarization-mediated glymphatic dysfunction in Parkinson's disease. J Adv Res. 2024;56:125–36.
25. Farrell JS, Wolff MD, Teskey GC. Neurodegeneration and pathology in epilepsy: clinical and basic perspectives. Adv Neurobiol. 2017;15:317–34.
26. Leal-Campanario R, Alarcon-Martinez L, Rieiro H, Martinez-Conde S, Alarcon-Martinez T, Zhao X, et al. Abnormal capillary vasodynamics contribute to ictal neurodegeneration in epilepsy. Sci Rep. 2017;7:43276.
27. Villa BR, Bhatt D, Wolff MD, Addo-Osafo K, Epp JR, Teskey GC. Repeated episodes of postictal hypoxia are a mechanism for interictal cognitive impairments. Sci Rep. 2023;13:15474.
28. Sun J, Zheng Y, Chen Z, Wang Y. The role of Na+ -K+ -ATPase in the epileptic brain. CNS Neurosci Ther. 2022;28:1294–302.
29. Jha RM, Kochanek PM, Simard JM. Pathophysiology and treatment of cerebral edema in traumatic brain injury. Neuropharmacology. 2019;145:230–46.
30. Simard JM, Kent TA, Chen M, Tarasov KV, Gerzanich V. Brain oedema in focal ischaemia: molecular pathophysiology and theoretical implications. Lancet Neurol. 2007;6:258–68.
31. Hong K-S, Cho Y-J, Lee SK, Jeong S-W, Kim WK, Oh EJ. Diffusion changes suggesting predominant vasogenic oedema during partial status epilepticus. Seizure. 2004;13:317–21.
32. Hatashita S, Hoff JT. Brain edema and cerebrovascular permeability during cerebral ischemia in rats. Stroke. 1990;21:582–8.
33. Erdlenbruch B, Alipour M, Fricker G, Miller DS, Kugler W, Eibl H, et al. Alkylglycerol opening of the blood-brain barrier to small and large fluorescence markers in normal and C6 glioma-bearing rats and isolated rat brain capillaries. Br J Pharmacol. 2003;140:1201–10.
34. Natah SS, Mouihate A, Pittman QJ, Sharkey KA. Disruption of the blood-brain barrier during TNBS colitis. Neurogastroenterol Motil. 2005;17:433–46.
35. Hoffman HJ, Olszewski J. Spread of sodium fluorescein in normal brain tissue. A study of the mechanism of the blood-brain barrier. Neurology. 1961;11:1081–5.
36. Malmgren LT, Olsson Y. Differences between the peripheral and the central nervous system in permeability to sodium fluorescein. J Comp Neurol. 1980;191:103–7.
37. Ahishali B, Kaya M. Evaluation of blood-brain barrier integrity using vascular permeability markers: Evans blue, sodium fluorescein, albumin-alexa fluor conjugates, and horseradish peroxidase. Methods Mol Biol. 2021;2367:87–103.
38. Nagelhus EA, Ottersen OP. Physiological roles of aquaporin-4 in brain. Physiol Rev. 2013;93:1543–62.
39. Mestre H, Hablitz LM, Xavier AL, Feng W, Zou W, Pu T, et al. Aquaporin-4-dependent glymphatic solute transport in the rodent brain. eLife. 2018;7:e40070.
40. Liu K, Zhu J, Chang Y, Lin Z, Shi Z, Li X, et al. Attenuation of cerebral edema facilitates recovery of glymphatic system function after status epilepticus. JCI insight. 2021;6:e151835.
41. Kim J-E, Yeo S-I, Ryu HJ, Kim M-J, Kim D-S, Jo S-M, et al. Astroglial loss and edema formation in the rat piriform cortex and hippocampus following pilocarpine-induced status epilepticus. J Comp Neurol. 2010;518:4612–28.
42. Sheen SH, Kim J-E, Ryu HJ, Yang Y, Choi K-C, Kang T-C. Decrease in dystrophin expression prior to disruption of brain-blood barrier within the rat piriform cortex following status epilepticus. Brain Res. 2011;1369:173–83.
43. Kwon HS, Koh S-H. Neuroinflammation in neurodegenerative disorders: the roles of microglia and astrocytes. Transl Neurodegener. 2020;9:42.
44. Shapiro LA, Wang L, Ribak CE. Rapid astrocyte and microglial activation following pilocarpine-induced seizures in rats. Epilepsia. 2008;49(Suppl 2):33–41.
45. Borges K, McDermott D, Irier H, Smith Y, Dingledine R. Degeneration and proliferation of astrocytes in the mouse dentate gyrus after pilocarpine-induced status epilepticus. Exp Neurol. 2006;201:416–27.
46. Farrell JS, Gaxiola-Valdez I, Wolff MD, David LS, Dika HI, Geeraert BL, et al. Postictal behavioural impairments are due to a severe prolonged hypoperfusion/hypoxia event that is COX-2 dependent. eLife. 2016;5:e19352.
47. Li E, d'Esterre CD, Gaxiola-Valdez I, Lee T-Y, Menon B, Peedicail JS, et al. CT perfusion measurement of postictal hypoperfusion: localization of the seizure onset zone and patterns of spread. Neuroradiology. 2019;61:991–1010.
48. Choy M, Wells JA, Thomas DL, Gadian DG, Scott RC, Lythgoe MF. Cerebral blood flow changes during pilocarpine-induced status epilepticus activity in the rat hippocampus. Exp Neurol. 2010;225:196–201.
49. de Vasconcelos AP, Bouilleret V, Riban V, Wasterlain C, Nehlig A. Role of nitric oxide in cerebral blood flow changes during kainate seizures in mice: genetic and pharmacological approaches. Neurobiol Dis. 2005;18:270–81.
50. Jespersen SN, Østergaard L. The roles of cerebral blood flow, capillary transit time heterogeneity, and oxygen tension in brain oxygenation and metabolism. J Cereb Blood Flow Metab. 2012;32:264–77.
51. Hablitz LM, Vinitsky HS, Sun Q, Stæger FF, Sigurdsson B, Mortensen KN, et al. Increased glymphatic influx is correlated with high EEG delta power and low heart rate in mice under anesthesia. Sci Adv. 2019;5:eaav5447.
52. Hickman S, Izzy S, Sen P, Morsett L, El Khoury J. Microglia in neurodegeneration. Nat Neurosci. 2018;21:1359–69.
53. Wen W, Cheng J, Tang Y. Brain perivascular macrophages: current understanding and future prospects. Brain. 2024;147:39–55.

Publisher's Note